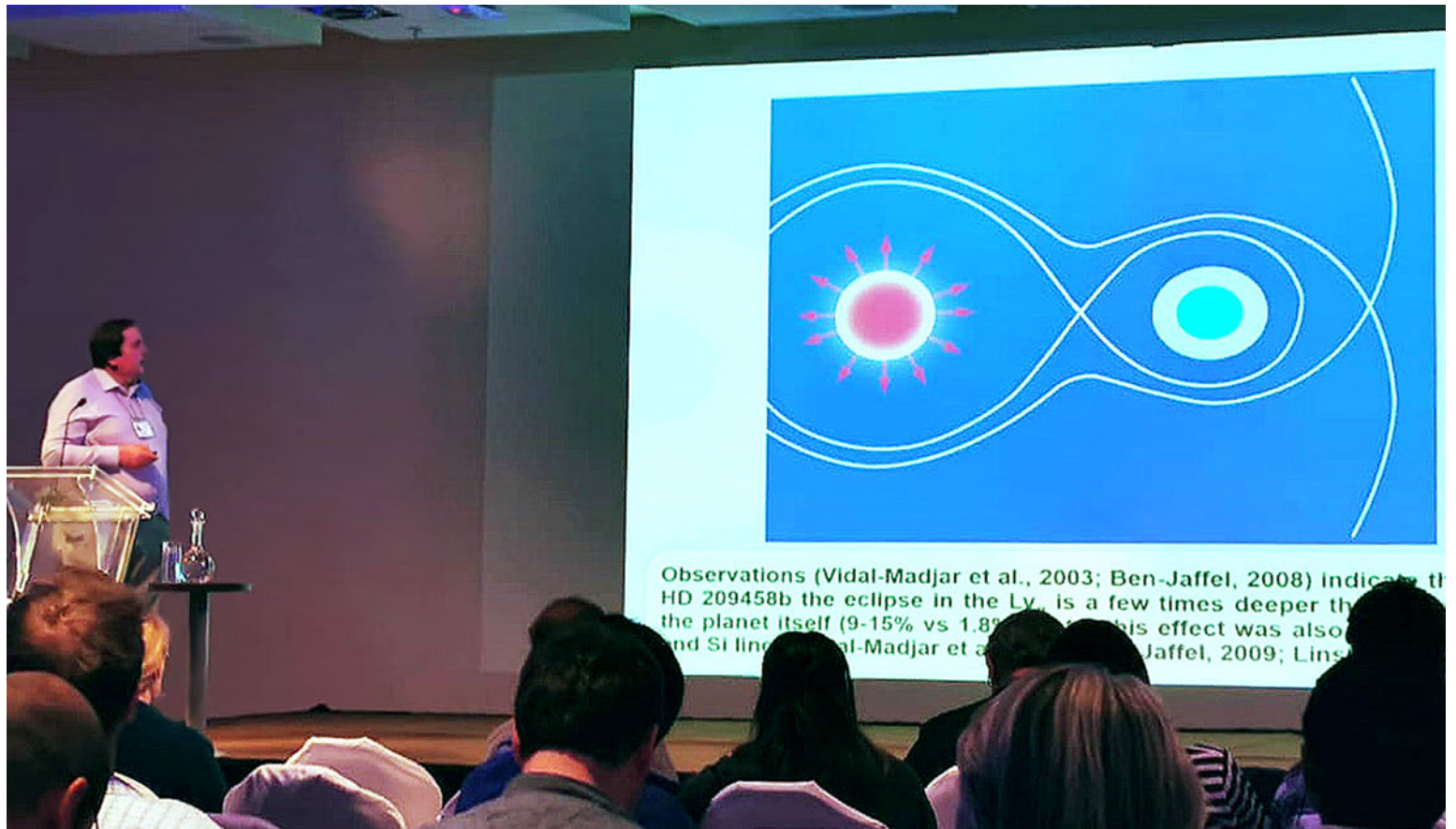


## Chapter 6. Star-planet relations



Dmitry Bisikalo

# Solar activity influences on planetary atmosphere evolution: Lessons from observations at Venus, Earth, and Mars

J. G. Luhmann 

Space Sciences Laboratory, University of California, Berkeley, CA 94720, USA  
email: [jgluhman@ssl.berkeley.edu](mailto:jgluhman@ssl.berkeley.edu)

**Abstract.** The Pioneer Venus and Venus Express missions, and the Mars Express and MAVEN missions, along with numerous Earth orbiters carrying space physics and aeronomy instruments, have utilized the increasing availability of space weather observations to provide better insight into the impacts of present-day solar activity on the atmospheres of terrestrial planets. Of most interest among these are the responses leading to escape of either ion or neutral constituents, potentially altering both the total atmospheric reservoirs and their composition. While debates continue regarding the role(s) of a planetary magnetic field in either decreasing or increasing these escape rates, observations have shown that enhancements can occur in both situations in response to solar activity-related changes. These generally involve increased energy inputs to the upper atmospheres, increases in ion production, and/or increases in escape channels, e.g. via interplanetary field penetration or planetary field ‘opening’. Problems arise when extrapolations of former loss rates are needed. While it is probably safe to suggest lower limits based simply on planet age multiplied by currently measured ion and neutral escape rates, the evolution of the Sun, including its activity, must be folded into these estimations. Poor knowledge of the history of solar activity, especially in terms of coronal mass ejections and solar wind properties, greatly compounds the uncertainties in related planetary atmosphere evolution calculations. Prospects for constraining their influences will depend on our ability to do a better job of solar activity history reconstruction.

**Keywords.** solar wind Interactions, solar activity, space weather effects

---

## 1. Introduction

Planetary atmospheric loss to space, often referred to as escape, is but one element in efforts to understand what led to the present conditions of each member of our solar system. Of special interest are the terrestrial planets within (or close to) the habitable zone. These both relate to our own circumstances here on Earth, and also continue to be discovered in increasing numbers among the extrasolar planets (e.g. [Tsiaras \*et al.\* 2019](#)), giving impetus to the search for life elsewhere. As a result, the trio of Venus, Earth and Mars has been subject to targeted investigations in the form of space exploration toward understanding the similarities and contrasts among the three, as well as implications for their past and future, and for other worlds. In particular, Mars currently has a relatively thin CO<sub>2</sub> atmosphere, with pressure roughly equivalent to what would be present if the Earth’s atmosphere started at stratospheric altitudes. Yet there is surface evidence suggesting an early atmosphere that had sufficient pressure to allow lakes, and perhaps even seas, to form (e.g. [Villanueva \*et al.\* 2015](#)). Alternatively, Venus has the atmospheric equivalent of Earth’s carbonate rocks present in gaseous form, forming a thick CO<sub>2</sub> atmospheric blanket that has produced a ‘runaway greenhouse’, hostile to familiar forms

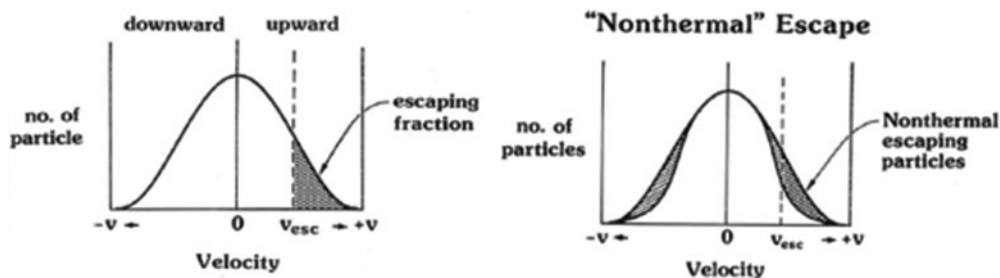


**Figure 1.** Illustrations of particle velocity distributions leading to Jeans or thermal escape (left), and its ‘non-thermal’ counterpart (right). In thermal escape, the distributions are described by Maxwell-Boltzmann functions, while in non-thermal escape, they depart from that behavior in many different ways that alter the distribution above the escape velocity, including the broadening at high energies suggested here, or even a shift to the right or left.

of life and even robotic explorers (Kasting 1988; Hall 2019). Yet this thick atmosphere is also largely devoid of water, as is the extremely hot surface. How did these planets and their atmospheres become so different, presuming they formed in roughly the same pre-planetary nebula around the Sun? Their respective distances from the Sun surely played some part, as did the smaller mass of Mars. But did their magnetic field histories also play a role? The different consequences of their photochemistry? More specifically, in light of the subject of this paper, did their atmospheric escape histories differ in ways that led to their present states?

One thing that is certain is that the Sun plays a dominating role in planetary atmosphere behavior through its effects on heating and atmospheric chemistry. Some of these effects are straightforward and concern the usual vaporization, thermalization, and photochemical processes. Others are less direct and often involve complex chains of different physical phenomena. But all essentially depend on the intensities and spectra of solar photon and particle emissions, which vary greatly with solar activity. Available observations now provide a good basic picture of some of these atmospheric energization processes, including their dependence on the planets’ seasons and solar activity cycle phase. Coupled with the expectation that the more active solar conditions must have prevailed early in the planets’ evolution, which is inferred from observations of Sun-like stars, these give further incentive for considering the long-term consequences of escape. On the threshold of new observations and rapidly expanding interests in terrestrial planet-star interactions, it is worth considering how well we understand the solar activity control of the current atmospheric losses to space, as well as identifying what more can be done to better constrain its impacts.

## 2. Escape processes

The basic physics of atmospheric escape is relatively simple: any process or chain of processes that energize some particles in a planetary atmosphere to speeds greater than the escape velocity  $v_{esc} = (2MG/r)^{1/2}$  ( $\sim 10\text{--}11$  km/ for Earth and Venus,  $\sim 5$  km/s for Mars) can lead to loss of constituents to space. Most of these losses occur from the upper terrestrial atmospheres, where the surface boundary layer and thermalizing collisions become rare. Escape processes may be ‘thermal’ or ‘nonthermal’, ‘bulk’ or ‘kinetic’, and often involve ionized species affected by electric and magnetic fields. Figure 1 illustrates a few of these. In thermal or ‘Jeans’ escape of neutral gas above the ‘exobase’, the altitude at which Venus, Earth and Mars atmospheres transition to a more collisionless behavior can be lost if they are outward-directed and not on ballistic or orbiting trajectories. This is due to density falloff with altitude, outward-bound particles belonging to the

typical Maxwell-Boltzmann velocity distribution above the escape speed. In this case, a hotter gas results in more escape. In the contrasting case of ‘non-thermal’ escape, some acceleration or energization process creates a non-Maxwellian distribution where the numbers of particles above the escape speed increase. Non-Maxwellian distributions can take many forms, and the processes leading to them may not affect the entire velocity distribution, as in the case illustrated here. However, as for the thermal process, the requirement for a particle’s leaving the planet is the same. If the species is ionized, the basic requirement regarding escape speed and trajectory are the same, but a host of new energization mechanisms comes into play. In fact, ionization is often a key factor in enabling significant escape, as described below in the context of our three planetary examples.

### 3. Contrasts between Venus, Earth, and Mars Escape

The present-day compositions of the Venus, Earth and Mars atmospheres tell part of the story of long-term atmospheric escape. As mentioned above, both Venus and Mars have CO<sub>2</sub>-dominated atmospheres that show a relatively extreme lack of water in their atmospheres and on their surfaces. In contrast, Earth’s air blanket is nitrogen-rich, in large part because its CO<sub>2</sub> content has been removed by our liquid water, which has transformed it to carbonate rocks (e.g. [Fegley 2014](#)). The focus of interest is thus often on H and O escape, and their role in determining a planet’s surface water. In particular, debate often centers on what role a planetary magnetosphere like Earth’s plays in ‘shielding’ the atmosphere from processes that lead to escape of these constituents. In exploring this still open question, potentially important information is available in the physics of current atmospheric loss at each of these bodies, apart from the thermal escape differences that are due to their different heliocentric locations.

Earth’s magnetospheric solar wind interaction converts the incident energy and momentum of the solar wind into a number of different forms. The solar wind convection electric field ( $E = -V_{sw} \times B$ ) maps into the high latitude ionosphere along open magnetic field lines, where it drives large-scale, cross-polar cap motion in the partially ionized upper atmosphere. The upper atmosphere there is the main reservoir for escape. Light hydrogen atoms undergo Jeans escape, but hydrogen ions also move outward along the ‘open’ magnetic field lines in the polar cusp and polar cap where interconnections between Earth’s magnetic field and the interplanetary field occur, as illustrated in [Figure 2a](#). This light ion ‘polar wind’, which also includes helium ions, is enabled by an ambipolar electric field that develops along the field lines due to gravitational separation of the oppositely charged heavier ion and light electron populations. Other energization of ions occurs in the magnetotail, where there is internal magnetospheric magnetic reconnection occurring as part of the magnetosphere’s global circulation. These dynamics lead to suprathermal electron precipitation in the auroral zone that heats and ionizes upper atmosphere neutrals, resulting in the upward acceleration of an ‘auroral wind’ of heavier ions, including O<sup>+</sup>. The details of the latter (see [Figure 2b](#)) appear to involve wave-particle interactions that add energy perpendicular to the locally vertical magnetospheric field, which is then converted by the magnetic mirror force to form upward moving, field-aligned ‘beams’ and ‘conic’ ion distributions with speeds greater than the escape speed. The efficiency, and thus effects, of this conversion, as well as the extent to which the outgoing O<sup>+</sup> is contained within the closed fields of the magnetosphere (e.g. as part of the ring current), versus escape on open field lines are still open questions.

If the upward-flowing ions eventually escape Earth, estimates of the flux based on their density  $\approx 10^5 \text{ cm}^{-3}$ , and velocity  $\approx 1 \text{ km/s}$ , give values  $\approx 10^{10} \text{ cm}^{-2}\text{s}^{-1}$ . When the area of the atmospheric footprint over which they are observed is considered, (e.g.,  $1000 \text{ km} \times 100 \text{ km}$ , based on global average precipitation maps such as that in [Figure 3a](#)), the

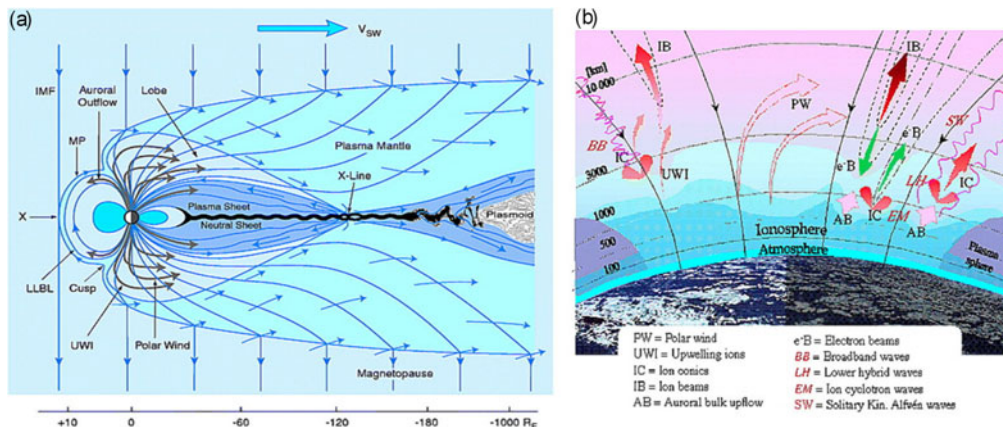


**Figure 2.** a) Illustration from Moore & Horwitz (2007) of the magnetic topology of the coupled solar wind-magnetosphere system (for Southward interplanetary field), showing the various ion flows within the system. Outflows from the high-latitude ionosphere can either escape to space along open magnetic field lines or enter the plasma sheet region of the magnetotail, where they either recirculate in the magnetosphere or are ejected as part of plasmoids resulting from the magnetotail reconnection processes. b) Illustration from Moore & Horwitz (2007) of the many plasma physical processes occurring in the high latitude ionosphere that can lead to ion energization and escape.

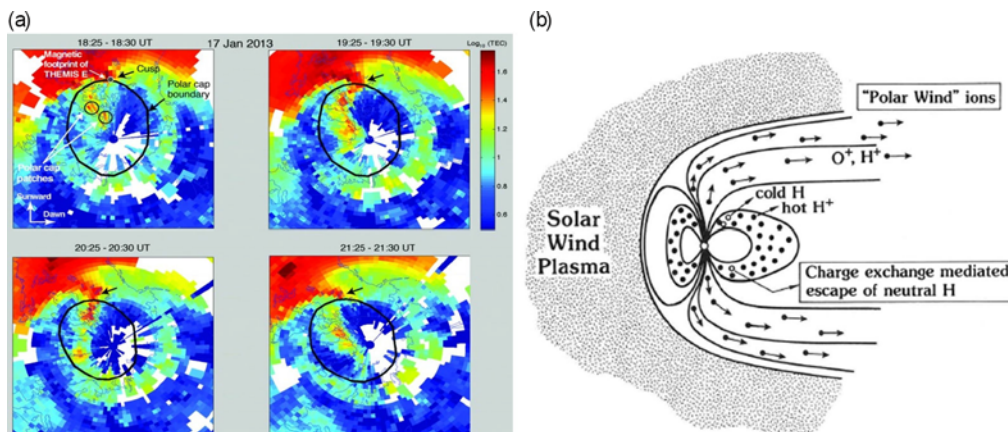


**Figure 3.** a) Illustration of the statistical footprints of electron precipitation inferred from high-latitude total electron content (TEC) obtained from GPS satellite transmissions (Walsh *et al.* 2014). Noon is at the top in these figures. The red tongue-like feature is the magnetospheric cusp location. b) Illustration of ion escape, including the closed field locations where charge exchange with ambient neutrals provides additional loss in the form of the produced energetic neutrals.

net outflow rate is  $\approx 10^{25} \text{ s}^{-1}$ . In addition, for the ions injected from below that are on closed field lines and contribute to the magnetospheric ring current (Figure 3b), charge exchange with high altitude neutral atoms of the primarily H exosphere leads to added non-thermal escape of the resulting energetic neutrals. This is especially important for H escape, with rates of up to  $\sim 10^{27}/\text{s}$  if limited by the rate of supply from below.

In contrast to the Earth, planetary magnetic fields do not prevent a direct solar wind interaction with the atmospheres at Venus and Mars, as can be seen by comparing Figure 3a with Figures 4a,b. The solar wind both upstream of the bow shock and in the magnetosheath around these planetary ‘obstacles’ penetrates into their neutral upper

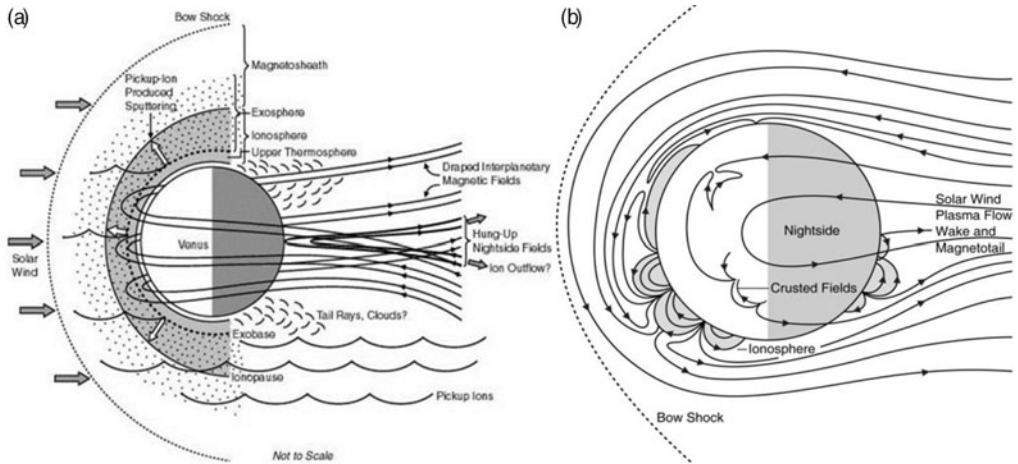


**Figure 4.** a) Illustration of the Venus-solar wind interaction; (b) The Mars solar wind interaction has the addition of crustal magnetic fields which add to the obstacles' and processes' complexities, but is in some basic ways, similar to the Venus case (reproduced from [Russell et al. 2016](#)).

atmospheres. As a result, atmospheric/ionospheric energization processes are different than at Earth. In addition, due to the scaling of these much smaller obstacles, both fluid-like and kinetic (test particle-like) processes come into play. For example, the solar wind convection electric field 'picks up' the ions produced in the region of overlap by photoionization, electron impact, or charge exchange with solar wind protons, as well as ions transported there from below. This process effectively 'mass loads', and thus further slows the solar wind plasma that is being deflected around Venus and Mars by combinations of ionospheric induced currents and (in the case of Mars) crustal magnetic fields, helping to create the highly draped fields of their comet-like induced magnetotails. But the gyroradii of the picked-up heavy (e.g.  $O^+$ ) ions can be comparable to, or larger than, the planetary radius, as illustrated in the left panel of Figure 4a and in Figure 5b, which show the Venus-solar wind interaction features. This leads to partial deposition of the energized planetary pickup ions back into the planets' upper atmospheres, with the possible outcome of additional neutral upper atmosphere losses by the sputtering process (e.g. see discussion in [Curry et al. 2015](#)). The field draping in the magnetosheath and magnetotail regions also exerts another force on the planetary ions, referred to as the magnetic tension force in Figure 5a. Also known as the magnetic 'slingshot' force, it sweeps up planetary ions where the ionosphere becomes denser and more fluid-like in its behavior. In addition, thermal ionosphere ion pressure gradients exist on the draped, penetrating magnetic fields that can accelerate upper atmosphere ions outward in a 'polar wind' like fashion (also indicated in Figure 5a).

Observations of planetary ions at both Venus and Mars are well-modeled, assuming the processes in Figure 5b are at work (see Figure 6, which show locations of energetic  $O^+$  ions detected on PVO around Venus, compared to a test particle picture of ion pickup in the region of atmosphere-solar wind overlap).

Similarly, the Mars Polar  $O^+$  Ion 'Plume', as observed on MAVEN (Figure 7a) and similarly modeled with test particles (Figure 7b), accounts for a significant fraction ( $\sim 30\%$ ) of Mars' total  $O^+$  escape ([Dong et al. 2015](#)). The lower-energy escaping ions in the solar wind wakes that occupy the Venus and Mars draped magnetotail 'plasma sheets' are generally considered to result from the magnetic tension force, while the thermal pressure gradient forces contribute additional outgoing ions both at and beyond the terminator

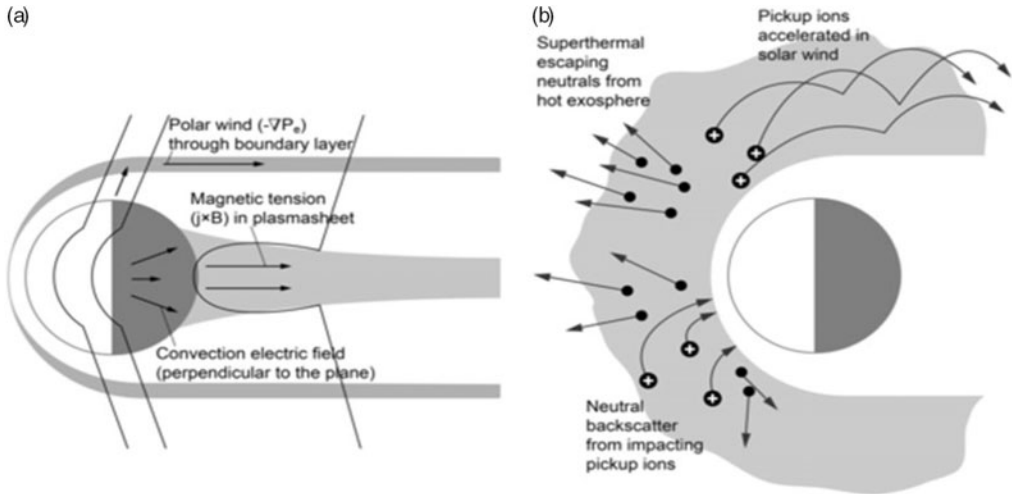


**Figure 5.** a) Illustration from [Futaana \*et al.\* \(2017\)](#) of the fluid-like processes involved in the escape of ions from Venus (and to some extent at Mars); (b) The other escape processes at Venus (and Mars) that involve the more kinetic aspects of their planetary ion behavior.

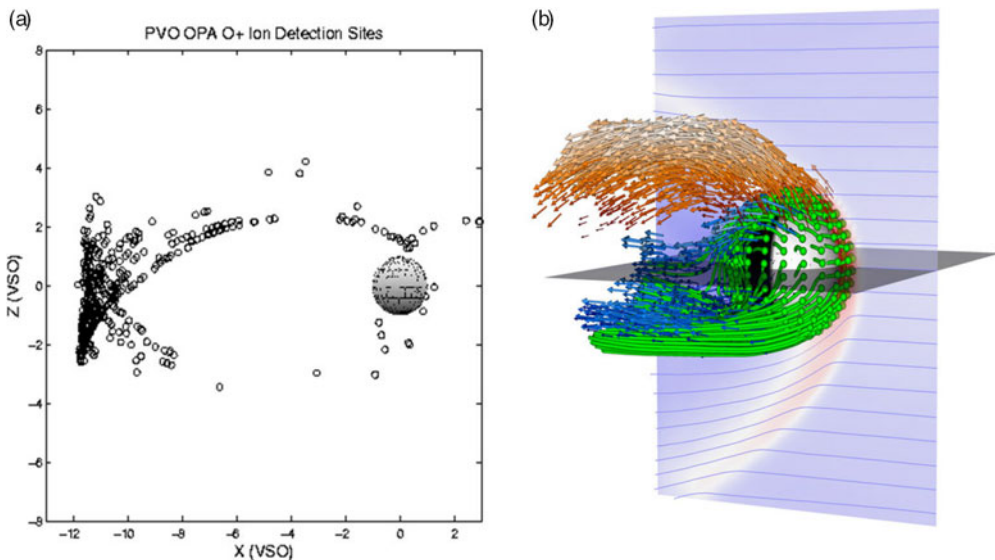


**Figure 6.** (a) Locations in the PVO orbit where O<sup>+</sup> pickup ions were observed (from [Luhmann \*et al.\* 2006](#)), compared to (b) a model of the picked up ions ([Jarvinen \*et al.\* 2010](#)). The locations of H<sup>+</sup> pickup ions are also shown here in blue.

(e.g. [Dubinin \*et al.\* 2017](#)). Mars' crustal fields are also thought to provide an additional loss mechanism associated with reconnection between the crustal fields and draped interplanetary fields ([Brain \*et al.\* 2010](#)), but the relative importance of that effect has yet to be evaluated, as does potential erosion associated with solar wind/ionosphere boundary shear-related instabilities (e.g., steepening Kelvin-Helmholtz waves ([Ruhunusiri \*et al.\* 2016](#))) and the typically time-dependent boundary conditions (e.g. from heliospheric current sheet/interplanetary field sector boundary crossings ([Edberg \*et al.\* 2011](#))). It has also been suggested that Venus ion loss can be affected by magnetic field reconnection

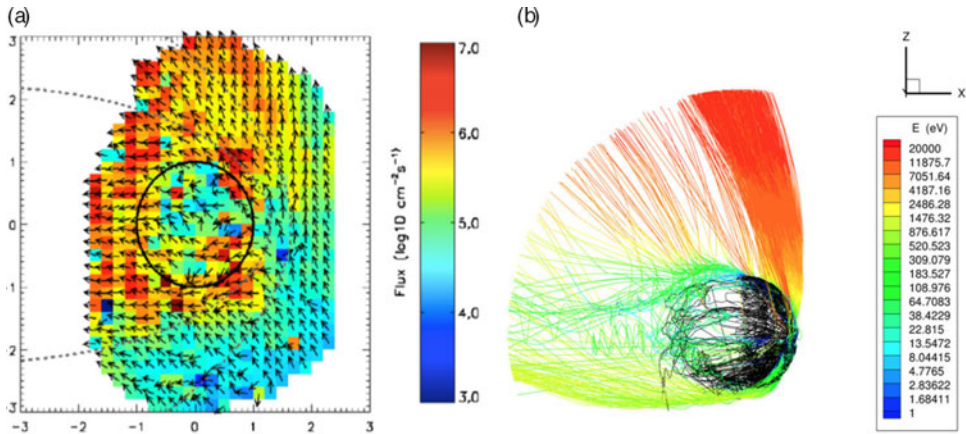


**Figure 7.** (a) MAVEN observations of escaping oxygen ions showing the statistical pattern of the fluxes, and the upward ‘plume’ extension in the coordinated system organized by the solar wind convection electric field (from Dong *et al.* 2015). (b) O+ test particles in a Mars’ solar wind interaction model, for a similar geometry with ion trajectories color-coded by their energies (Fang *et al.* 2008).

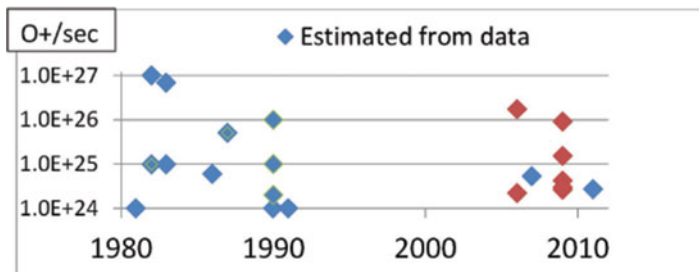


**Figure 8.** Figure illustrating previous estimates of Venus O+ escape rates, based on both measurements (blue) and models (red), from McEnulty (2012).

across its draped magnetotail lobes, when it occurs close to the planet (Zhang *et al.* 2012).

Ion escape rate estimates from some of these additional processes have been attempted. For example, from PVO ionospheric ‘cloud’ measurements (ionospheric ions seen in the magnetosheath adjacent to the main ionosphere), Brace *et al.* (1982) arrived at the number  $7 \times 10^{26}$  ions/sec, based on measured transit times, probability of occurrence, statistical distribution, and average electron density. Meanwhile, Russell *et al.* (1982) inferred  $2 \times 10^{25}$  ions/sec loss during one cloud event, assuming a similar cloud in the south. These are significant compared to estimates/measurements of escape via the other processes at Venus. In general, escape rate estimates (in Figure 8, adapted from McEnulty 2012) show that Venus O+ escape rates versus the year of published estimate vary by orders of magnitude (blue indicates those derived from observations, red indicates those derived from models).

The primarily CO<sub>2</sub> atmospheres also have a photochemical channel for neutral O escape, which is especially important at Mars. The reaction  $\text{CO}_2^+ + \text{O} \rightarrow \text{O}_2^+ + \text{CO}$ , followed by dissociative recombination  $\text{O}_2^+ + e \rightarrow \text{O}^* + \text{O}^*$ , proceeds rapidly in Venus’ and Mars’ ionospheres. This photochemical process produces ‘hot O coronas’ around both planets. The energies of some of these hot atoms are  $>2$  eV, which puts them above the lower escape velocity for Mars, though not for Venus, where  $\sim 10$  eV is required. This

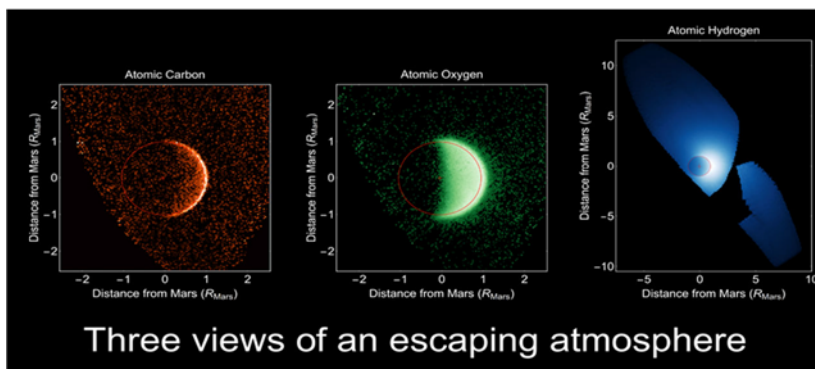


**Figure 9.** The upper C, O, and H atmospheres of Mars, as observed on MAVEN prior to its orbital insertion (from [Schneider \*et al.\* 2015](#)).

|  | H Jeans                         | O ion              | O Dissoc<br>Recomb | O sputtering       |
|--|---------------------------------|--------------------|--------------------|--------------------|
| Present-day loss rate from<br>MVN ( $s^{-1}$ ) | $1.6\text{--}11 \times 10^{26}$ | $5 \times 10^{24}$ | $5 \times 10^{25}$ | $3 \times 10^{24}$ |
| 4.2 b.y. at present rate, $H_2O$               | 3.6–25.2 m                      | 0.2 m              | 2.2 m              | 0.14 m             |
| 4.2 b.y. at present rate, $CO_2$               |                                 | 6 mbar             | 68 mbar            | 4 mbar             |

**Figure 10.** Rates of escape and associated equivalent global amounts of water and  $CO_2$  loss over time ( $\sim 3.5$  Gyr) for Mars, based on measurements by MAVEN. (Adapted from [Jakosky \*et al.\* 2018](#)).

process also increases  $O^+$  escape, even for Venus, by putting more O at higher altitudes, where it can be ionized and picked up in the magnetosheath and solar wind. A similar process also works for C loss at Mars (e.g. [Hu \*et al.\* 2015](#)). MAVEN observations of atomic C, O and H coronas, as seen in [Figure 9](#), have allowed new escape rate estimates to be made for these neutral constituents. Also, it has been found that the H corona, with its escaping component, is probably enhanced by dust storm activity (e.g. [Chaffin \*et al.\* 2014](#)).

To evaluate the overall impacts of all of these processes, e.g. for water loss, one needs to add the different escape rates for H and O, as recently done for Mars by [Jakosky \*et al.\* \(2018\)](#) (see [Figure 10](#)):

The current atmospheric escape rates at all three planets are too low to explain inferred losses of evolutionary interest. For example, the estimated volume of an early ocean of Mars is  $\sim 6 \times 10^7 \text{ km}^3 H_2O$  (from surface features). This amount contains about  $2 \times 10^{45} H_2O$  molecules. It is relatively easy to lose the light hydrogen by extra (e.g. EUV) heating. But to remove the oxygen in this ocean over a few Gyr requires an average loss rate of at least  $\sim 10^{28} O$  atoms/s (over 100 times greater than present rates).

#### 4. Escape Enhancers

The Sun produces, in addition to its varying EUV outputs, flares, enhanced solar wind flows and fields, coronal transients, and solar energetic particles (SEPs). The two kinds of solar wind structures that produce the greatest solar wind and SEP enhancements are illustrated in [Figure 11](#). The interplanetary coronal mass ejections (ICMEs) that produce

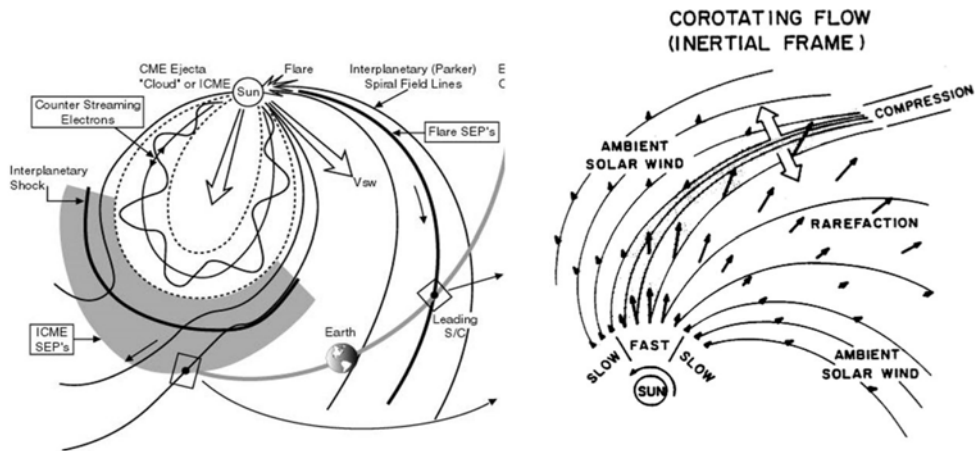


**Figure 11.** (Left panel) Illustration of an interplanetary coronal mass ejection's (ICME's) effects on the solar wind and interplanetary magnetic field, including solar wind compression/pileup ahead of it that is sometimes preceded by a shock (from [Luhmann et al. 2008](#)). (Right panel) Illustration of the effect of interacting solar wind streams, which result in spiral-shaped compressions that can appear to rotate with the Sun (from [Pizzo 1978](#)).

the greatest effects under the present solar conditions (left panel) result from erupting coronal structures that occur most often around the solar cycle maximum phase, while solar wind stream interactions (right panel) occur throughout the cycle. The ICME produces a number of different effects on planetary space environments. First, the largest events are often initiated around the time of a flare on the Sun, which is then closely followed in some cases by the arrival of high energy particles, mainly protons and electrons, accelerated in the corona. Concurrently, the ejection of coronal material occurs, traveling at speeds up to nearly 4-5 times the typical solar wind speed. This ICME structure plows through the ambient corona and solar wind, piling up the density and magnetic field, and for fast ejections, producing a leading interplanetary shock, which provides a source of more energetic particles that speed ahead of it throughout its several-day transit times to reach these planets. Then the planetary interaction reacts to the shock, the compressed solar wind behind it, and the usually stronger than average and sometimes highly inclined magnetic fields of the coronal material, which is sometimes well-described as a large flux rope of a few tenths of an AU (in a cross section). This entire sequence from the flare to the coronal ejecta passage can last several days, as illustrated in Figure 12.

Passage of ICMEs can greatly enhance the overall magnetospheric ion energization, precipitation, and outflow processes. The Earth's auroras during and following solar activity provide a measure of the energy deposited in the atmosphere and its spatial extent. Related ion outflow rates follow suit, showing dependence on disturbance parameters such as incident solar wind pressure (see Figure 13).

The Venus electron density altitude profiles in Figure 14 illustrate its much different, more direct dayside ionosphere boundary response to enhanced solar wind pressure, which arrives with the leading compressed solar wind portion of the ICME event. In addition to the inferred erosion of the topside ionosphere, the overlying draped magnetosheath field is both present at lower altitudes, and penetrates into the ionosphere. Mars exhibits its own version of this consequence, in that its crustal fields show increasing degrees of open topologies due to enhanced reconnection with these penetrating fields ([Xu et al. 2018](#)).

Associated diffuse auroral emissions, examples of which are shown in Figure 15, are seen on the night sides of both Venus and Mars ([Phillips et al. 1986](#); [Schneider et al. 2015, 2018](#)). These occur in coincidence with the local enhancements of SEPs, which,

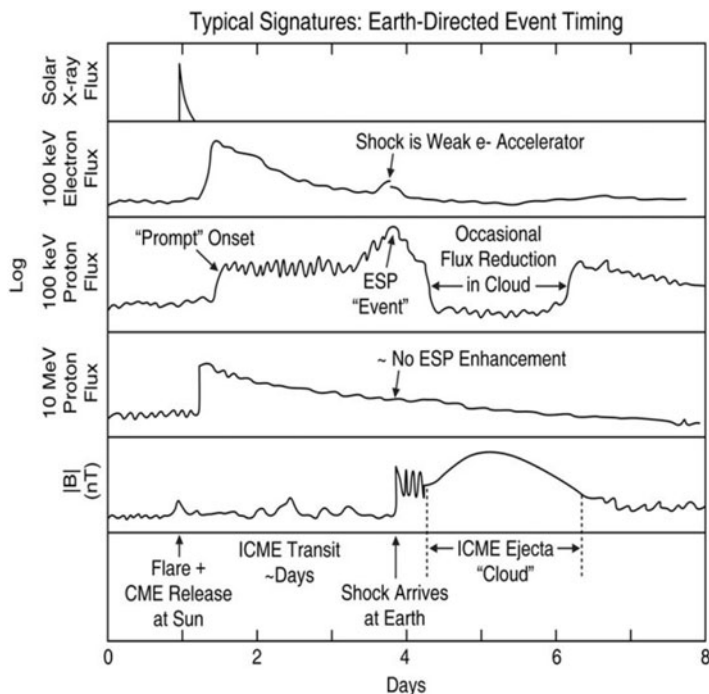


**Figure 12.** The different phenomena and timing of events associated with ICMEs result in a range of effects in planetary space environments. Here, a ‘classic’ time series of observations (solar X-rays and in-situ particles and fields) around the time of a major ICME event illustrates a particular sequence that occurs with a ‘direct’ impact (see Figure 11, left panel).

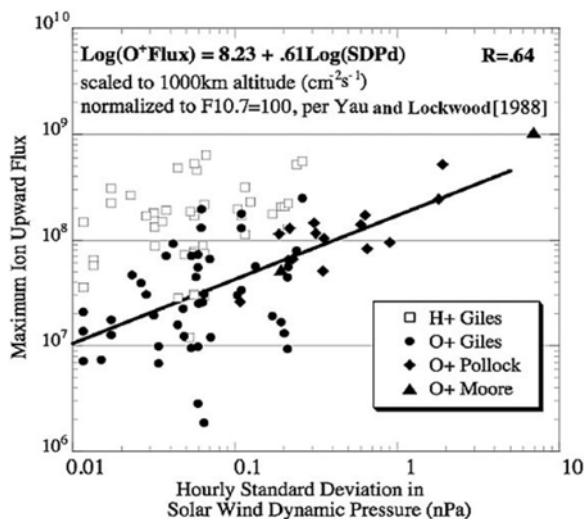


**Figure 13.** Figure from Moore & Horwitz (2007) showing the intensification of outflowing hydrogen and oxygen ions in the Earth’s polar regions in response to increases in solar wind pressure.

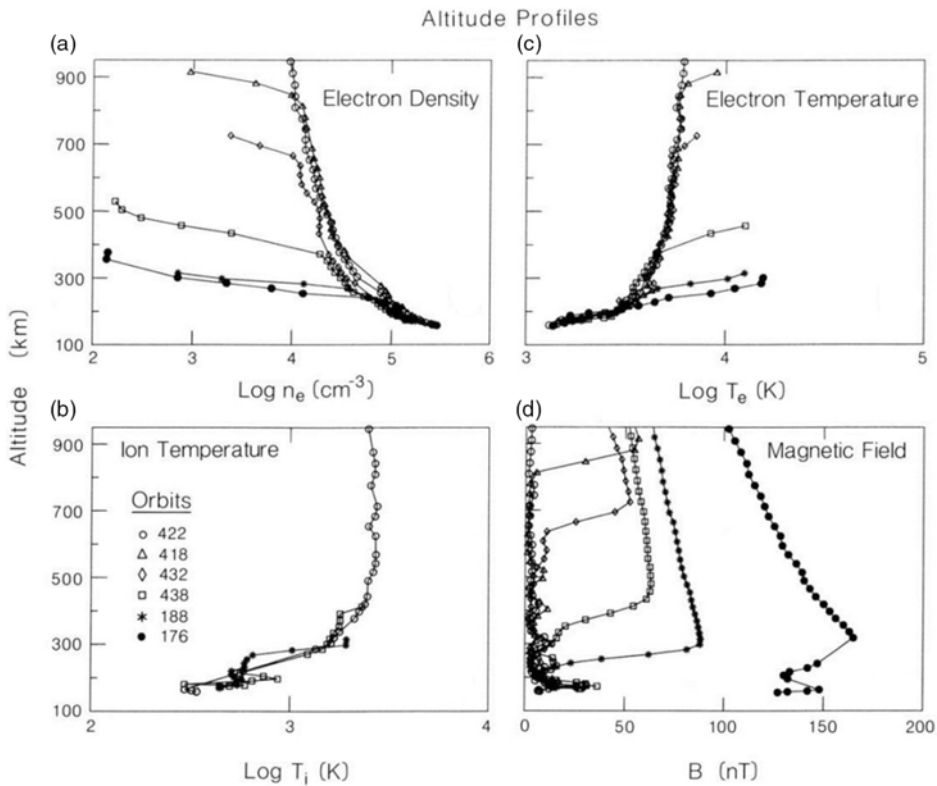


**Figure 14.** PVO dayside ionospheric density altitude profiles selected to illustrate their dependence on the incident solar wind pressure. In particular, the increasing solar wind erosion of the topside ionosphere is seen in the top left plot, while the corresponding lowering of the overlying magnetosheath and penetration of the magnetic field into the ionosphere is seen in the lower right plot. (From [Luhmann \*et al.\* 1987.](#))

as mentioned above, can precede the ICME shock arrival by days and last throughout the event, sometimes peaking in intensity at the shock arrival (see Figure 12). Venus auroral emissions in the visible green line have also been seen from the ground in the days following coronagraph observations of Venus-directed CMEs ([Gray \*et al.\* 2014.](#))

[Lee \*et al.\* \(2018\)](#) summarize the details of how Mars responded to a significant ICME impact witnessed by MAVEN instruments in the form of the time series in Figure 16. Upper atmosphere heating and expansion briefly occurs in response to the flare, but the SEPs and their effects can be present for days, because the shock that travels outward ahead of the ICME is a relatively long-lasting source that populates a large swath of heliosphere in front of and around it with SEPs. The access of these ionizing particles to the lower atmosphere is enhanced by the observation that the crustal magnetic fields open up in response to solar wind compression and increased external field penetration. The enhanced magnitude of the external field also plays a role in this access. Whether atmospheric escape is significantly impacted by such events is to be determined.

Because spacecraft observations are restricted to the few orbits occurring prior to and during ICME passage, which cover only a small portion of the Mars-solar wind interaction space, MHD simulation results for the events ([Ma \*et al.\*](#)) are used to obtain a global picture and the related global escape rates ([Ma \*et al.\*, 2017;](#) [Dong \*et al.\*, 2015.](#)) Figure 17 shows snapshots of meridional Mars planetary ion flux contours ( $\log \text{flux (cm}^{-2} \text{ s}^{-1})$ )

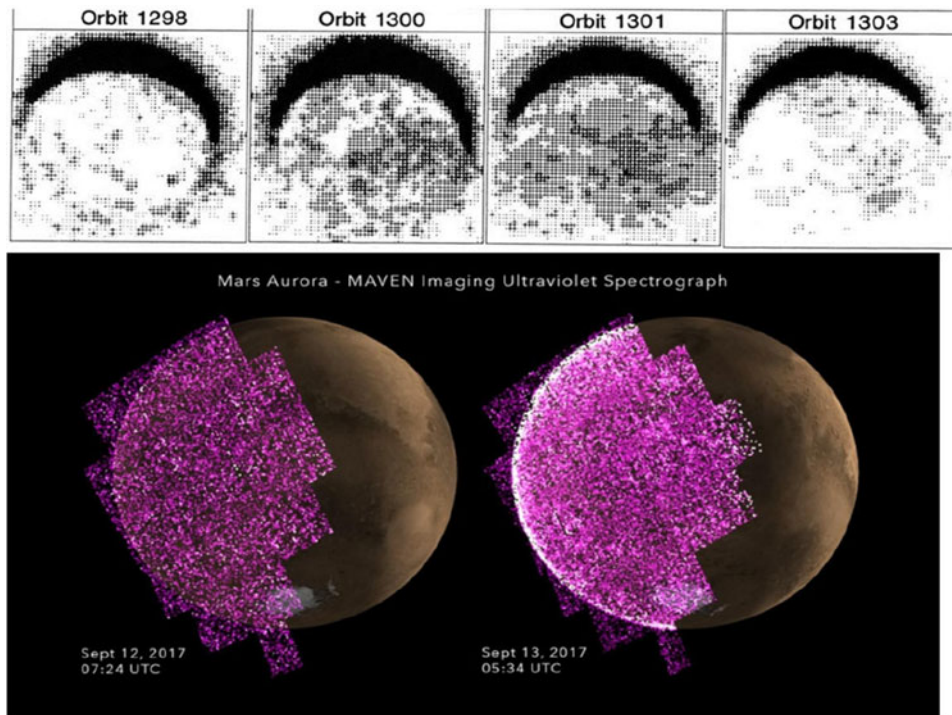


**Figure 15.** (Top) PVO UV images showing, in negative shading, the brightening of a diffuse nightside aurora seen in the 130.4 nm spectral line (from Phillips *et al.* 1986). (Bottom) MAVEN UV images of an auroral brightening at Mars that accompanied a SEP event and ICME impact (Schneider *et al.*, 2017).

before and during the event from the simulation, where the effect of the ICME passage is clearly seen. The estimated global ion escape in this case changed  $\sim 10\times$  from  $10^{24}$  ions/s to  $10^{25}$  ions/s. During the MAVEN mission, the encountered solar events have been relatively moderate. Had Mars experienced an ‘extreme’ ICME event such as that observed on the STEREO A spacecraft in 2012 (e.g. Liu *et al.*, 2013), similar model results suggest the global ion escape rate would have increased to  $10^{27}$  ions/s. PVO was in orbit around Venus during a much stronger solar cycle, and experienced larger and more frequent events. PVO  $> 36$  eV and anti-sunward ion data (see Figure 18) suggest Venus O<sup>+</sup> escape rates increased during ICMEs by 100x or more (Luhmann *et al.*, 2007).

## 5. Effects over time

The challenge of reconstructing the history and consequences of these effects requires many assumptions involving poorly constrained conditions. Nonetheless, such exercises help identify specific gaps that new observables can sometimes fill. It is most straightforward to start calculations  $\sim 3.5$ -3.8 Gyr ago, rather than at 4.5 Gyr, when solar system formation processes, including impacts, were still at work (e.g. Jakosky *et al.*, 2019), and to assume that today’s planetary magnetic fields were already established. This also limits the effects of recently uncovered uncertainties in solar EUV history (Tu *et al.* 2015), based on observations of the range of EUV emitted by hundreds of G-type stars, including fast and slow rotators, as in Figure 19. It is currently unknown where the solar EUV evolution track falls, leaving up to an order of magnitude uncertainties for up to a third of the Sun’s main sequence life.

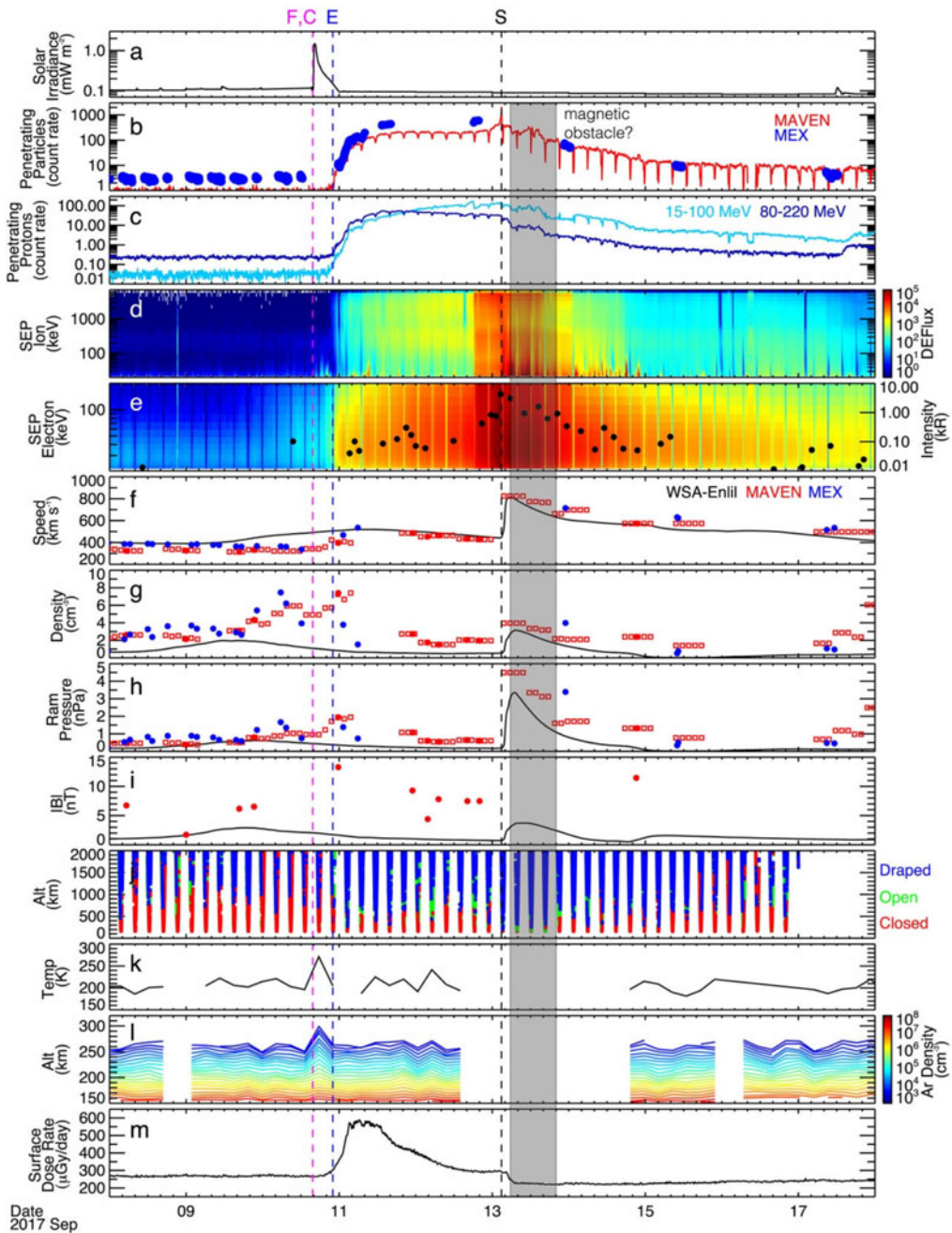


**Figure 16.** A time series of diverse observations from MAVEN, Mars Express and MSL, showing details of how Mars responded to a significant ICME impact in September 2017 (from [Lee et al. 2018](#)). The panels show (from the top), the solar flare in EUV intensity, the SEPs (including electrons and ions), the solar wind plasma parameters (density, velocity, temperature), and the magnetic field, all showing the shock arrival, a color bar indicating the change of local magnetic topology (red = closed fields, blue = open fields), and the upper atmosphere temperature and density response. The bottom panel is the highest energy SEP signature from MSL RAD on the surface. While these observations show that many different ICME responses occur at Mars, estimates of the related changes in globally escaping planetary ion flux require complementary modeling.

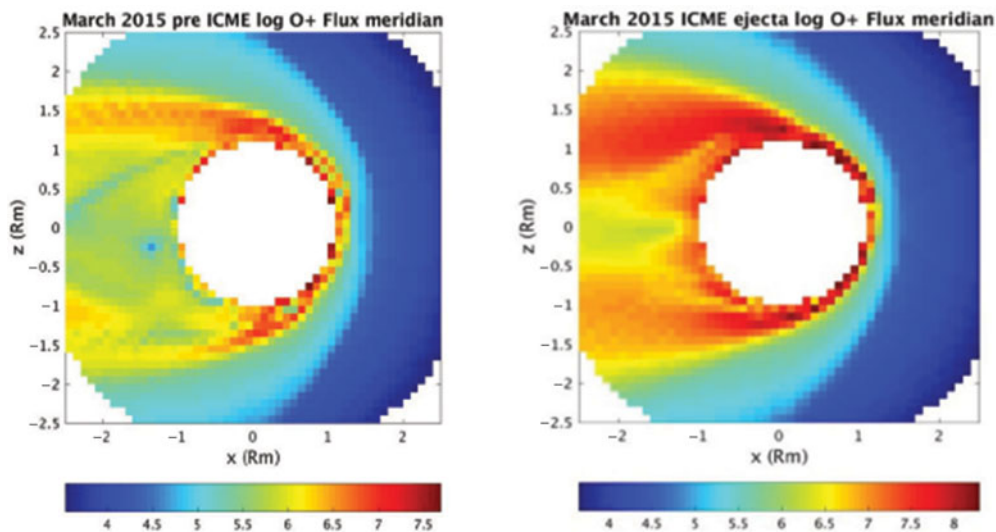


**Figure 17.** Meridian contours of planetary ion fluxes around Mars based on a data-validated model of an ICME passage in March 2015 (Ma *et al.* 2017; Luhmann *et al.* 2017). These represent snapshots of the conditions before the ICME arrived (left panel), and during the period when the coronal ejecta was present (right), illustrating the global enhancement of the escaping ion fluxes.

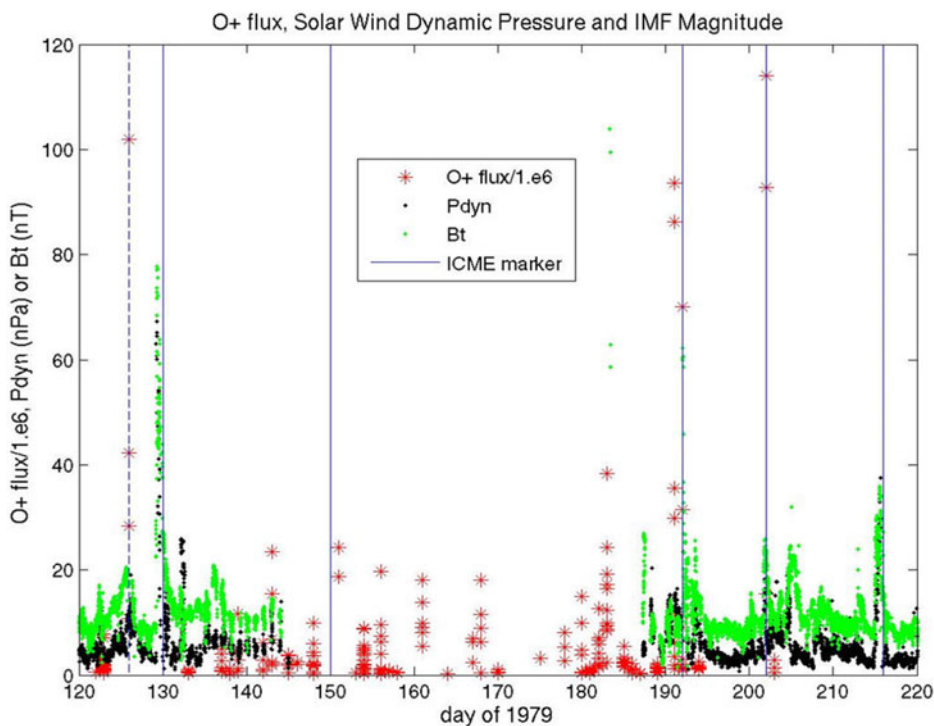


**Figure 18.** Extended timeline comparing escaping suprathermal planetary ion fluxes observed on PVO with the incident solar wind dynamic pressure ( $P_{\text{dyn}}$ ) and interplanetary magnetic field (IMF) strength ( $B_t$ ) at the time. The inferred escaping fluxes increase by up to  $\sim 100\times$  during periods of high  $P_{\text{dyn}}$  and  $B_t$ , which are associated with solar wind inter-stream compression regions and ICMEs. (From Luhmann *et al.* 2007.)

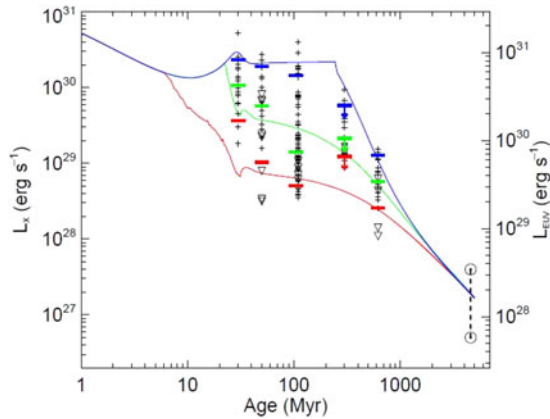


**Figure 19.** Figure from [Tu \*et al.\* \(2015\)](#), illustrating the range of possible EUV histories of Sun-like stars, depending on their rotational histories.

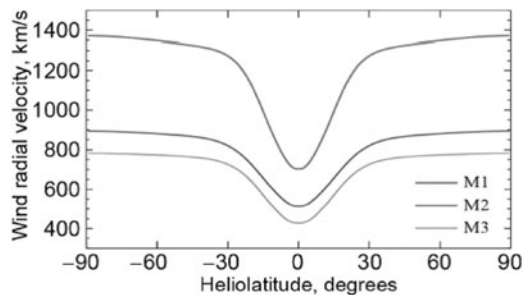


**Figure 20.** This figure from [Airapetain & Usmanov \(2016\)](#) shows models for solar wind velocities for the present-day Sun (M3), and for solar ages of 2.0 Gyr (M2) and 0.7 Gyr (M1).

Even less constrained are early solar wind models (e.g. see [Wood \*et al.\* 2015](#)). A recent model by [Airapetain & Usmanov \(2016\)](#) has conditions in its early epoch (see Figure 20, curve labeled M1), as extreme as today's observed ICME events. This early solar wind would have had major 'impacts' by itself.

## 6. Summary

It probably does not matter much if a planet is magnetized or not. Rather, the history of the solar and interplanetary conditions can determine atmospheric evolution in post-impact and post-hydrodynamic outflow-dominated escape epochs. We must better constrain them from times of about 1 Gyr of age. While Sun-like star observations are valuable, our Sun's own history is of utmost importance. Is the answer to be found at the moon, where samples may contain evidence of the early solar wind and solar activity? Kepler mission observations of 'superflares' on Sun-like stars of various ages ([Shibayama \*et al.\* 2013](#)) include flare energies of  $\sim 10^{34}$  ergs or more, compared to large present-day solar flares that have up to  $10^{32}$  ergs. The work of [Aarnio \*et al.\* \(2011\)](#) suggests that the empirical relationship between solar CME size (from coronagraphs) and solar flare intensity may apply to flaring Sun-like stars. But CMEs at these flaring early 'Suns' have been difficult to identify (e.g. [Osten & Wolk 2016](#)). Further observations are key to investigating this and other pertinent questions about both early solar wind and solar activity, and the planetary consequences they left behind.

## Acknowledgments

The work described in this review paper is based largely on results from NASA's PVO, MAVEN and MSL missions and ESA's Venus and Mars Express missions. The author is also supported by a NASA grant (for related space weather observations and modeling as part of the STEREO mission science team effort).

## References

- Aarnio, A. N., Stassun, K.G., Hughes, W.J., McGregor, S.L. 2011. Solar Flares and Coronal Mass Ejections: A Statistically Determined Flare Flux – CME Mass Correlation. *Sol. Phys.* 268, 195–212.
- Airapetain V. S., Usmanov, A.V. 2016 Reconstructing the Solar Wind from Its Early History to Current Epoch. *ApJL*. 817. doi:[10.3847/2041-8205/817/2/L24](https://doi.org/10.3847/2041-8205/817/2/L24).
- Brace, L.H., Theis, R.F., Hoegy, W.R. 1982. Plasma clouds above the ionopause of Venus and their implications. *Planet. Space Sci.* 30, 29–37, doi:[10.1016/0032-063390069-1](https://doi.org/10.1016/0032-063390069-1).
- Brain, D. A., Baker, A. H., Briggs, J., Eastwood, J. P., Halekas, J. S., and Phan, T.D. 2010. Episodic detachment of Martian crustal magnetic fields leading to bulk atmospheric plasma escape, *Geophys. Res. Lett.*, 37, L14108. doi:[10.1029/2010GL043916](https://doi.org/10.1029/2010GL043916).
- Chaffin, M. S., Chaufray, J.Y., Stewart, I., Montmessin, F., Schneider, N. M., and Bertaux, J.L. 2014. Unexpected variability of Martian hydrogen escape. *Geophys. Res. Lett.*, 41, 314–320, doi:[10.1002/2013GL058578](https://doi.org/10.1002/2013GL058578).
- Curry, S.M., Luhmann, J.G., Ma, Y.J., Liemohn, M., Dong, C., Hara, T. 2015. Comparative pick-up ion distributions at Mars and Venus: Consequences for atmospheric deposition and escape. *Planet. Space Sci.* 115, 35, 47.
- Dong, Y., Fang, X., Brain, D. A., McFadden, J. P., Halekas, J. S., Connerney, J. E., Curry, S. M., Harada, Y., Luhmann, J. G., Jakosky, B. M. 2015, Strong plume fluxes at Mars observed by MAVEN: An important planetary ion escape channel. *Geophys. Res. Lett.*, 42, 8942– 8950, doi:[10.1002/2015GL065346](https://doi.org/10.1002/2015GL065346).
- Dong, C., Ma, Y., Bougher, S. W., Toth, G., Nagy, A. F., Halekas, J. S., Dong, Y., Curry, S. M., Luhmann, J. G., Brain, D., *et al.* 2015, Multi-fluid MHD study of the solar wind interaction with Mars' upper atmosphere during the 2015 March 8th ICME event. *Geophys. Res. Lett.* 42, 9103– 9112, doi:[10.1002/2015GL065944](https://doi.org/10.1002/2015GL065944).
- Dubinin, E., Fraenz, M., Pätzold, M., McFadden, J., Halekas, J. S., DiBraccio, G. A., Zelenyi, L. 2017. The effect of solar wind variations on the escape of oxygen ions from Mars through different channels: MAVEN observations. *J. Geophys. Res. Space Phys.*, 122, 11285–11301. doi:[10.1002/2017JA024741](https://doi.org/10.1002/2017JA024741).
- Edberg, N. J. T., *et al.* 2011. Atmospheric erosion of Venus during stormy space weather. *J. Geophys. Res.* 116, A09308.
- Fang, X., Liemohn, M. W., Nagy, A. F., Ma, Y., De Zeeuw, D. L., Kozyra, J. U., Zurbuchen, T. H. 2008, Pickup oxygen ion velocity space and spatial distribution around Mars. *J. Geophys. Res.* 113, A02210, doi:[10.1029/2007JA012736](https://doi.org/10.1029/2007JA012736).
- Fegley, B., Jr. 2014. Venus. In H. D. Holland, & K. K. Turekian (Eds.), *Treatise on Geochemistry*, 2nd ed., vol. 2 (pp. 127–148). Amsterdam, Netherlands: Elsevier.
- Futaana, Y., Stenberg Wieser, G., Barabash, S., *et al.* 2017. Solar Wind Interaction and Impact on the Venus Atmosphere, *Space Sci. Rev.* 212, 1453. doi:[10.1007/s11214-017-0362-8](https://doi.org/10.1007/s11214-017-0362-8).
- Gray, C.L., Chanover, N.J., Slinger, T.G., Molaverdikhani, K. 2014. The effect of solar flares, coronal mass ejections, and solar wind streams on Venus' 5577Å oxygen green line. *Icarus*. 233, 342–347. doi:[10.1016/j.icarus.2014.01.029](https://doi.org/10.1016/j.icarus.2014.01.029).
- Hall, S. 2019. Venus is Earth's evil twin - and space agencies can no longer resist its pull. *Nature*. 570, 20–25. doi:[10.1038/d41586-019-01730-5](https://doi.org/10.1038/d41586-019-01730-5).
- Hu, R., Kass, D., Ehlmann, B. *et al.* 2015. Tracing the fate of carbon and the atmospheric evolution of Mars. *Nat. Comm.* 6, 10003. doi:[10.1038/ncomms10003](https://doi.org/10.1038/ncomms10003).

- Jakosky, B. Brain, D., Chaffin, M., Curry, S., Deighan, J., Grebowsky, J., Halekas, J., Leblanc, F., Lillis, R., Luhmann, J.G. *et al.* 2018. Loss of the Martian atmosphere to space: Present-day loss rates determined from MAVEN observations and integrated loss through time. *Icarus*. 315, 146–157. doi:[10.1016/j.icarus.2018.05.030](https://doi.org/10.1016/j.icarus.2018.05.030).
- Jarvinen, R., Kallio, E., Dyadechkin S., *et al.* 2010. Widely different characteristics of oxygen and hydrogen ion escape from Venus. *Geophys. Res. Lett.* 37, L16201. doi:[10.1029/2010GL044062](https://doi.org/10.1029/2010GL044062).
- Kasting, J. F. 1988. Runaway and moist greenhouse atmospheres and the evolution of Earth and Venus. *Icarus*, 74, 472–494.
- Lammer, H., Kasting, J. F., Chassefière, E., *et al.* 2008. Atmospheric escape and evolution of terrestrial planets and satellites. *Space Sci. Rev.* 139, 399–436. doi:[10.1007/s11214-008-9413-5](https://doi.org/10.1007/s11214-008-9413-5).
- Lee, C. O., Jakosky, B. M., Luhmann, J. G., Brain, D. A., Mays, M. L., Hassler, D. M., *et al.* 2018. Observations and impacts of the 10 September 2017 solar events at Mars: An overview and synthesis of the initial results. *Geophys. Res. Lett.* 45, 8871– 8885. <https://doi.org/10.1029/2018GL079162>.
- Liu, Y., Luhmann, J., Kajdič, P. *et al.* 2014. Observations of an extreme storm in interplanetary space caused by successive coronal mass ejections. *Nat Comm.* 5, 3481. doi:[10.1038/ncomms4481](https://doi.org/10.1038/ncomms4481).
- Luhmann, J. G., *et al.* 2017, Martian magnetic storms. *J. Geophys. Res. Space Physics*. 122, 6185– 6209, doi:[10.1002/2016JA023513](https://doi.org/10.1002/2016JA023513).
- Luhmann, J.G., Curtis, D.W., Schroeder, P. *et al.* 2008. STEREO IMPACT Investigation Goals, Measurements, and Data Products Overview. *Space Sci. Rev.* 136, 117. doi:[10.1007/s11214-007-9170-x](https://doi.org/10.1007/s11214-007-9170-x).
- Luhmann, J. G., Kasprzak, W. T., and Russell, C. T. 2007, Space weather at Venus and its potential consequences for atmosphere evolution. *J. Geophys. Res.* 112, E04S10. doi:[10.1029/2006JE002820](https://doi.org/10.1029/2006JE002820).
- Luhmann, J.G., Ledvina, S.A., Lyon, J.G., Russell, C.T. 2006. Venus O+ pickup ions: Collected PVO results and expectations for Venus Express. *Planet. Space Sci.* 54, 1457–1471, doi:[10.1016/j.pss.2005.10.009](https://doi.org/10.1016/j.pss.2005.10.009).
- Luhmann, J. G., Russell, C. T., Scarf, F. L., Brace, L. H., and Knudsen, W. C. 1987. Characteristics of the Marslike limit of the Venus-solar wind interaction. *J. Geophys. Res.* 92 (A8), 8545– 8557. doi:[10.1029/JA092iA08p08545](https://doi.org/10.1029/JA092iA08p08545).
- Ma, Y. J., *et al.* 2017. Variations of the Martian plasma environment during the ICME passage on 8 March 2015: A time-dependent MHD study. *J. Geophys. Res. Space Physics*. 122, 1714– 1730, doi:[10.1002/2016JA023402](https://doi.org/10.1002/2016JA023402).
- McEnulty, T. 2012. Oxygen Loss from Venus and the Influence of Extreme Solar Wind Conditions, PhD thesis, University of California, Berkeley. <https://www.worldcat.org/title/oxygen-loss-from-venus-and-the-influence-of-extreme-solar-wind-conditions/oclc/842823603>.
- Moore, T. E., Horwitz J. L. 2007. Stellar ablation of planetary atmospheres. *Rev. Geophys.* 45, RG3002. doi:[10.1029/2005RG000194](https://doi.org/10.1029/2005RG000194).
- Osten, R., Wolk, S. 2016. A Framework for Finding and Interpreting Stellar CMEs. *Proceedings of the International Astronomical Union*, 12(S328), 243–251. doi:[10.1017/S1743921317004252](https://doi.org/10.1017/S1743921317004252).
- Phillips, J. L., Stewart, A. I. F., Luhmann, J. G. 1986. The Venus ultraviolet aurora: Observations at 130.4 nm. *Geophys. Res. Lett.* 13, 1047–1050, doi:[10.1029/GL013i010p01047](https://doi.org/10.1029/GL013i010p01047).
- Pizzo, V. J. 1978. A Three-Dimensional Model of Corotating Streams in the Solar Wind - I. Theoretical Foundations. *J. Geophys. Res.* 83, 5563–5572.
- Ruhunusiri, S., *et al.* 2016, MAVEN observations of partially developed Kelvin-Helmholtz vortices at Mars. *Geophys. Res. Lett.* 43, 4763– 4773. doi:[10.1002/2016GL068926](https://doi.org/10.1002/2016GL068926).
- Russell, C.T., Luhmann, J.G., Strangeway, R.J. 2016. *Space Physics: An Introduction*, Cambridge University Press.
- Russell, C. T., Luhmann, J. G., Elphic, R. C., Scarf, F. L. and Brace, L. H. 1982. Magnetic field and plasma wave observations in a plasma cloud at Venus. *Geophys. Res. Lett.* 9, 45–48. doi:[10.1029/GL009i001p00045](https://doi.org/10.1029/GL009i001p00045).

- Schneider, N. M., Jain, S. K., Deighan, J., Nasr, C. R., Brain, D. A., Larson, D., *et al.* 2018. Global aurora on Mars during the September 2017 space weather event. *Geophys. Res. Lett.*, 45, 7391–7398. <https://doi.org/10.1029/2018GL077772>.
- Schneider, N. M., Deighan, J. I., Jain, S. K., Stiepen, A., Stewart, A. I. F., Larson, D., Mitchell, D. L., Mazelle, C., Lee, C. O., Lillis, R. J., Evans, J. S., Brain, D., Stevens, M. H., McClintock, W. E., Chaffin, M. S., Crismani, M., Holsclaw, G. M., Lefevre, F., Lo, D. Y., Clarke J. T., Montmessin, F., Jakosky, B.M. 2015. Discovery of diffuse aurora on Mars. *Science*. 350, doi:[10.1126/science.aad0313](https://doi.org/10.1126/science.aad0313).
- Shibayama, T., Maehara, H., Notsu, S., Notsu, Y., Nagao, T., Honda, S., Ishii, T., Nogami, T., Daisaku, T., Kazunari, S. 2013. Superflares on Solar-type Stars Observed with Kepler. I. Statistical Properties of Superflares. *ApJ Supp.* 209.
- Tsiaras, A., Waldmann, I.P., Tinetti, G. *et al.* 2019. Water vapour in the atmosphere of the habitable-zone eight-Earth-mass planet K2-18 b. *Nat Astron.* doi:[10.1038/s41550-019-0878-9](https://doi.org/10.1038/s41550-019-0878-9).
- Tu, L., Johnstone, C.P., Guedel, M., Lammer, H. 2015. The extreme ultraviolet and X-ray Sun in Time: High-energy evolutionary tracks of a solar-like star, *Astron. Astrophys.* 577, doi:[10.1051/0004-6361/201526146](https://doi.org/10.1051/0004-6361/201526146).
- Villanueva G. L., Mumma, M. J., Novak, R. E., Käufel, H. U., Hartogh, P., Encrenaz, T., Tokunaga, A., Khayat, A., Smith, M. D. 2015. Strong water isotopic anomalies in the Martian atmosphere: Probing current and ancient reservoirs, *Science* 348. 218–221. doi:[10.1126/science.aaa3630](https://doi.org/10.1126/science.aaa3630), 2015.
- Walsh, B. M., Foster, J. C., Erickson, P. J., Sibeck, D. G. 2014. Simultaneous Ground- and Space-Based Observations of the Plasmaspheric Plume and Reconnection. *Science*. 343, 1122–1125, doi:[10.1126/science.1247212](https://doi.org/10.1126/science.1247212). Jarvinen, R., Kallio, E., Dyadechkin S., *et al.* 2010. Widely different characteristics of oxygen and hydrogen ion escape from Venus. *Geophys. Res. Lett.* 37, L16201. doi:[10.1029/2010GL044062](https://doi.org/10.1029/2010GL044062).
- Wood, B.E., Linsky, J.L., Güdel, M. 2015. Stellar Winds in Time. In: Lammer H., Khodachenko M. (eds) *Characterizing Stellar and Exoplanetary Environments*. Astrophysics and Space Science Library, 411. Springer.
- Xu, S. *et al.* 2018. Investigation of Martian Magnetic Topology Response to 2017 September ICME, *Geophys. Res. Lett.*, 45, 7337–7346. doi:[10.1029/2018GL077708](https://doi.org/10.1029/2018GL077708)
- Zhang, T.-L. *et al.* 2012. Magnetic reconnection in the near Venusian magnetotail. *Science*. 336, 567–570.

## Discussion

DMITRY BISIKALO: Could you kindly comment on the role of the planetary magnetic field in the mass loss?

JANET LUHMANN: Observations suggest that for the most extreme external conditions, the presence of the field may not matter. The planetary magnetic field may not be able to prevent energization and losses, although it may change the detailed physics of the processes involved. The escape rates may ultimately depend on the atmospheric production and delivery (e.g. by photochemistry and diffusion) of species to regions from which they can escape (e.g. the exobase).